C. R. Chimie 21 (2018) 547–552

Contents lists available at ScienceDirect

Comptes Rendus Chimie

www.sciencedirect.com

Full paper/Mémoire

Aurivillius family of layered perovskites, $BiREWO_6$ (RE = La, Pr, Gd, and Dy): Synthesis, characterization, and photocatalytic studies

Srinivas Mamidi, Ravi Gundeboina, Sreenu Kurra, Radha Velchuri, Vithal Muga*

Department of Chemistry, Osmania University, Hyderabad 500 007, Telangana, India

ARTICLE INFO

Article history:
Received 30 October 2017
Accepted 30 January 2018
Available online 5 March 2018

Keywords:
Layered perovskites
X-ray diffraction
FT-IR
SEM
Band gap energy
Photocatalysis
Photoluminescence

ABSTRACT

The present work deals with the synthesis, characterization, and photocatalytic studies of layered perovskites belonging to Aurivillius family. Layered perovskites of various chemical compositions, $BiREWO_6$ (RE = La, Pr, Gd, and Dy), were synthesized by an ethylene glycol–assisted sol–gel method. These materials were characterized by X-ray diffraction, scanning electron microscopy–energy dispersive spectroscopy (EDS), Fourier transform infrared, Raman, and ultraviolet–visible diffuse reflectance techniques. The composition of all these materials was obtained from EDS. The unit cell lattice parameters were attained from Rietveld refinement program, Fullprof.2k, by refining the d-lines of $BiREWO_6$. The band gap energy of these samples was obtained from the Kubelka–Munk plot. The photocatalytic activity of all the samples was evaluated by photodegradation of methylene blue. The mechanistic degradation pathway of methylene blue was studied using radical quenchers.

1. Introduction

The organic dyes are extensively used in textiles, food, cosmetics, paper, leather industries, and so forth. A large quantity of these dyes is released into aquatic systems during their use. Most of these dyes are chemically stable and often inhibit the penetration of sunlight causing a reduction in the photosynthesis of submerged plants. Furthermore, a few nitrogen-containing dyes degrade in the presence of sunlight and release carcinogenic byproducts. Thus, these organic dyes cause massive damage to the ecosystem. The treatment of wastewater containing organic dyes by advanced oxidation processes using semiconducting photocatalysts is one of the economically viable processes adopted by a majority of scientists. Semiconductors such as TiO_2 and ZnO have been extensively investigated as photocatalysts, but their usage is limited due to their wide band gap energy. In view of environmental pollution and energy conservation, there is a need to develop new visible active semiconductors to effectively harvest sunlight, which is abundant and consists of about 45% of visible light. Recently, a few materials such as $BiVO_4$ [1,2], Bi_2WO_6 [3], Ag_3PO_4 [4,5], Ag_3VO_4 [6–8], and so on have shown promising visible light photoactivity.

Bismuth-containing materials belonging to Aurivillius family of layered perovskites such as Bi_2WO_6, Bi_2MoO_6, and $BiYWO_6$ have been found to have a superior photocatalytic activity to (1) split water completely into H_2 and O_2 and (2) degrade organic pollutants into innocuous CO_2 and H_2O [9–12]. In bismuth-containing oxides, for instance, $Bi_2Ti_2O_7$, theoretical calculations have shown that $6s^2$ of Bi^{3+} helps in reducing the band gap energy [13]. Furthermore, studies on partial density of state have revealed that Bi^{3+} helps in the enhancement of "p" character of the conduction band (note that the valence band of

* Corresponding author.
E-mail address: mugavithal@gmail.com (V. Muga).

https://doi.org/10.1016/j.crci.2018.01.011
1631-0748/

bismuth titanium oxides have good p character due to the contribution of oxygen 2p). These two factors of Bi^{3+} synergistically assist in upshifting the valence band leading to a decrease in band gap energy. Thus, Bi^{3+}-containing oxides or Bi^{3+}-doped materials are considered as broad-spectrum absorption photocatalysts [13,14] . In the present investigation, we have attempted to prepare Aurivillius family of layered perovskites of various chemical compositions, $BiREWO_6$ (RE = La, Pr, Gd, and DY), by the sol–gel method and studied their visible light photocatalytic activity.

2. Materials and methods

2.1. Preparation of $BiREWO_6$

Analytical grade bismuth nitrate, rare earth oxides, and tungsten metal powder were used as sources of Bi, Ln, and W, respectively. Stoichiometric amounts of $Bi(NO_3)_3$, RE_2O_3 (RE = La, Gd, and Dy), Pr_6O_{11} (for $BiPrWO_6$), and W corresponding to 3 g of the final product ($BiREWO_6$) were taken. $Bi(NO_3)_3$ was dissolved in dilute nitric acid (solution A). Rare earth oxide was converted to its nitrate by dissolving in dilute nitric acid and slowly evaporated to expel the excess nitric acid. The dried RE-nitrate was dissolved in 20 mL of distilled water (solution B). Tungsten metal was dissolved in 30% H_2O_2 solution (solution C). Solutions B and C were slowly added to solution A with constant stirring. The resultant mixture solution was converted into metal citrates by adding citric acid in the molar ratio of citric acid/metal ion 2:1 and, the pH of the solution was adjusted to 6–7 by adding dilute ammonia solution. The gelating reagent, ethylene glycol (EG), was added (molar ratio of metal/EG, 1:1.2). The contents were slowly heated on a hot plate. The transparent solution slowly turned into viscous solution first and then into the black paste like gel. The gel was dried and ground into fine powder (called precursor) and heated to 700 °C for 6 h in a muffle furnace in air and cooled naturally.

2.2. Characterization

The phase identification of the materials was examined by powder X-ray diffraction (PXRD) measurement using Cu Kα radiation λ = 1.5406 Å (Rigaku Miniflex-600, 40 kV, 20 mA). The PXRD pattern was obtained at room temperature using the fixed time mode over an angular step size of 2θ = 0.02° and scan step time of 0.15 s in the 2θ range 5°–80°. The energy dispersive spectra were recorded using the HITACHI SU-1500 variable pressure scanning electron microscope. A JASCO V-650 ultraviolet–visible (UV–vis) spectrophotometer was used for UV–vis diffuse reflectance spectra measurements in the range 200–900 nm. $BaSO_4$ was used as the reflectance standard. Raman spectra were recorded using a 632.81 nm line from a He–Ne laser, and the scattered light was analyzed using Horiba Jobin Yvon HR800. The laser was focused on a spot of ~3 μm and a 10× lens was used for the collection of back-scattered Raman signal. Infrared spectra were recorded in the form of KBr pellets in the wavenumber range 1000–400 cm^{-1} using a JASCO IR-5300 spectrometer.

The photocatalytic activity of the as-prepared $BiREWO_6$ (RE = La, Pr, Gd, and Dy) samples was evaluated by degradation of methylene blue (MB) under visible light irradiation at room temperature. Annular type photoreactor, model HVAR1234 (Heber Scientific, Chennai, India), equipped with a 300 W tungsten lamp (380–840 nm) was used. The lamp was placed inside the quartz tube. The temperature of the quartz tube was maintained at 27–30 °C by circulating cold water using a pump. The reaction mixture was prepared by adding 50 mg of the photocatalyst to 50 mL of a MB aqueous solution of concentration 10^{-5} mol L^{-1}. A glass tube of ~37 cm length and 2.5 cm diameter was used for placing the reaction mixture. The distance between the lamp and reaction vessel was ~5 cm. About 50 mL of the reaction mixture was placed in the reaction vessel and the suspension was stirred in the dark for 1 h to attain adsorption equilibrium. A blank experiment (dye solution without the catalyst) was also carried out. Subsequently, all reaction vessels were irradiated with visible light with constant air bubbling. About 4 mL of the reaction mixture was collected at regular 30 min time intervals and centrifuged to remove the catalyst particles. The supernatant solution was subjected to optical absorption measurements at 664 nm using a UV–vis spectrometer. The degradation amount of dyes can be calculated from the equation $d = (C_0 - C_i)/C_0$, where C_i is the concentration of MB solution at a time, t, in the process of photodegradation and C_0 is the initial concentration of MB.

To investigate the mechanistic degradation pathway of a dye molecule in the presence of the as-prepared materials, controlled photocatalytic experiments using different radical scavengers were also carried out under similar experimental conditions.

An additional experiment was also carried out to support the formation of $^{\cdot}OH$ radicals during photocatalysis under visible light irradiation. Typically, 0.05 g of the sample was suspended in 50 mL of a 0.02 M NaOH solution containing 3 mM terephthalic acid (TA). The suspension was stirred in the dark for 60 min, followed by visible light (300 W tungsten lamp) illumination. Then, 4 mL of the suspension was taken out at 60 min intervals, filtered, and recorded its fluorescence spectra using a JASCO FP-8500 spectrofluorometer. It is well known that the photogenerated $^{\cdot}OH$ radicals react with TA to form 2-hydroxyterephthalic acid (TAOH), which shows a characteristic fluorescence band centered at 426 nm. The increase in the fluorescence intensity is directly proportional to the concentration of photogenerated $^{\cdot}OH$ radicals. The measurement was carried out at the excitation wavelength of 320 nm.

3. Results and discussion

The simplest member of the Aurivillius family, Bi_2WO_6, is known to have three polymorphic phases: tetragonal, orthorhombic, and monoclinic. At room temperature, it adopts the orthorhombic structure, consisting of alternating fluorite-like $[Bi_2O_2]^{2+}$ layers and $[MO_4]^{2-}$ layers comprising corner-linked octahedral units, whereas at the high-temperature, it has a monoclinic structure (Fig. 1), retains the layered nature but the $[MO_4]^{2-}$ layers comprise

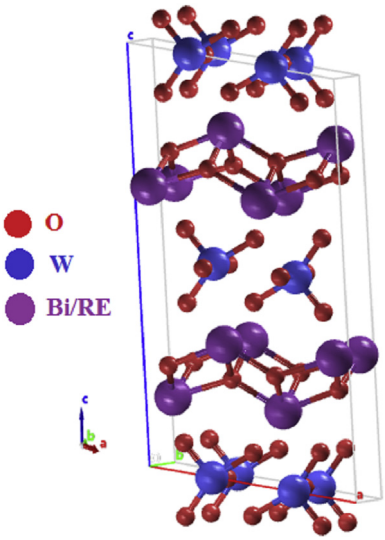

Fig. 1. Schematic structure of $BiREWO_6$.

edge-linked chains of octahedra [15]. Recently, it is reported that $BiREWO_6$ (RE = trivalent rare earth ions) structure is isotypic to the high-temperature Bi_2WO_6 (H-Bi_2WO_6) structure. However, rare earth–doped Bi_2WO_6 derivatives exhibit disorder around the octahedral site whereas Bi_2WO_6 does not. It has been suggested that the octahedral disorder is simply due to localized bonding competition at the Bi/Ln sites [15].

Santha et al. have prepared $BiREWO_6$ (RE = La, Nd, Pr, Gd, Sm, Tb, Yb, Y, and Dy) by the solid-state method in the temperature range 925–1000 °C depending on the rare earth oxide used [15]. To our knowledge, the method of preparation of these samples by EG-assisted sol–gel technique, structural investigation of $BiPrWO_6$ and their photocatalytic activity have not been reported. The precursors of these oxides were calcined at 700 °C for 6 h each and subjected to PXRD measurements for structural characterization. The X-ray diffraction (XRD) patterns of all samples are shown in Fig. 2a. The similarity in the PXRD patterns of these materials with that of monoclinic Bi_2WO_6 lattice was observed. Remarkably, the XRD peak positions exhibit a variation with the substitution of rare earth from La to Dy (Fig. 2b). This implies that the lattice parameters vary when the La atom is replaced by Pr, Gd, and Dy. The rare earth dependence crystalline structure of $BiREWO_6$ is also reported by Berdonosov et al. (RE = Y, Dy, Gd, Sm, Nd, and La) [16]. The change in unit cell parameters of isostructural crystal lattices depends on their respective ionic radius of cations/anions. The ionic radius of these ions effects the 2θ (or d-lines) position in the XRD patterns. According to Bragg's law, the increase (or decrease) in the d-value should result in the decrease (or increase) in lattice parameters. All the powder patterns were subjected to Rietveld analysis using Fullprof.2k software to obtain the lattice parameters. It is reported that the $BiREWO_6$ oxides (RE = Y, Nd, and Gd) [16–20] are isostructural to H-Bi_2WO_6 [21]. Hence, the structural parameters of H-Bi_2WO_6 were given as initial parameters for the refinement of XRD data of $BiREWO_6$ samples (crystallography open database ID: 1528731). It was found that the XRD pattern of all these oxides can be satisfactorily fitted within the space group $A12/m1$. The observed and calculated powder profiles of $BiREWO_6$ are shown in Fig. 3 (RE = Pr) and supporting information (Fig. S1 (RE = La), Fig. S2 (RE = Gd), and Fig. S3 (RE = Dy)). The lattice and fitting parameters of $BiREWO_6$ are given in Table S1. The variation in the lattice parameters was in good agreement with the above discussion.

The scanning electron microscopy images are represented in Fig. S4. It was observed that the morphology of $BiREWO_6$ was not uniform. $BiGdWO_6$ consists of agglomerated small crystallites having dimensions of 2 μm. Rest of the samples have agglomerated surface with small pores. The EDS analyses of all the samples were carried out in various parts of the sample. EDS can be used as a guideline for qualitative elemental analysis only. The results obtained from EDS are semiquantitative and are given Table S2.

The Fourier transform infrared (FT-IR) techniques are used to ascertain the local structure of the oxides. It is well known that the $BiREWO_6$ oxides give characteristic FT-IR

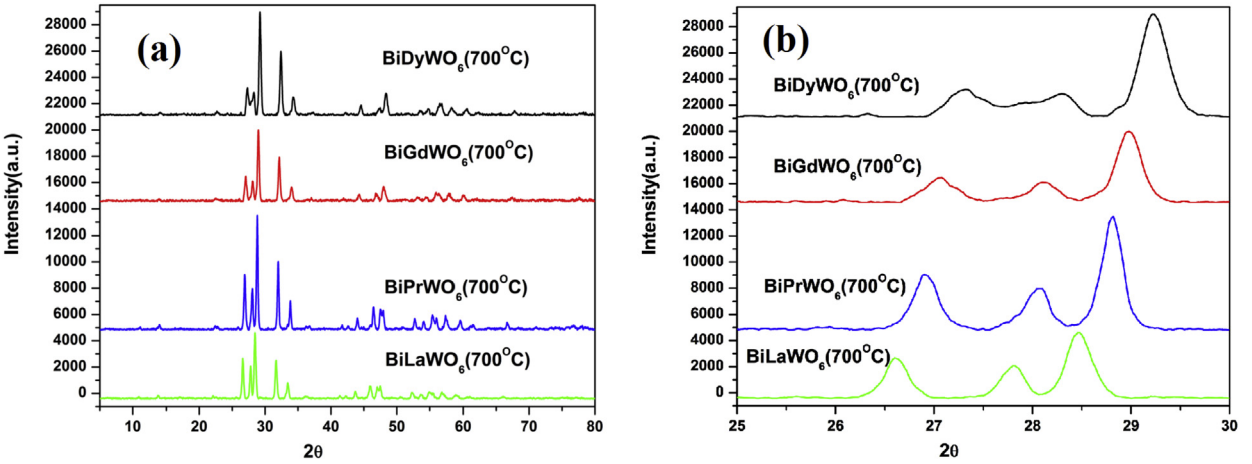

Fig. 2. (a) XRD patterns of $BiREWO_6$ (RE = La, Pr, Gd, and Dy) and (b) shift in the XRD patterns of $BiREWO_6$ (RE = La, Pr, Gd, and Dy).

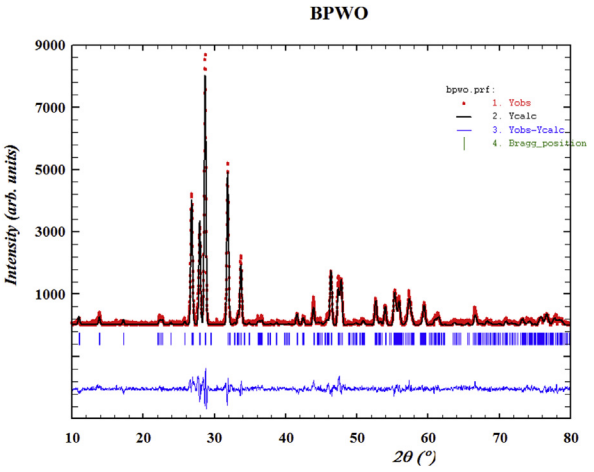

Fig. 3. The observed and calculated powder patterns of $BiPrWO_6$ (BPWO).

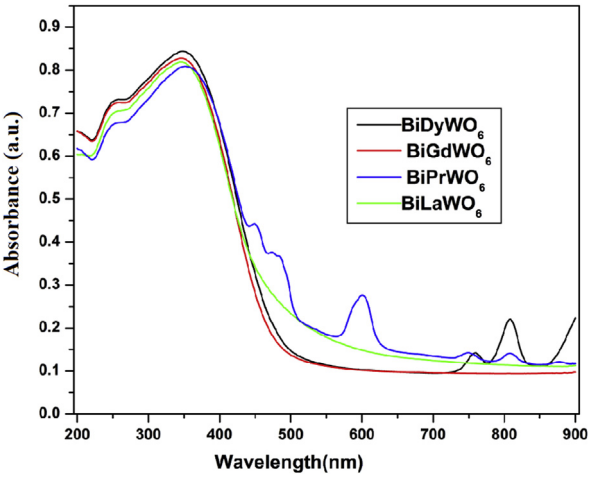

Fig. 4. Absorption spectra of $BiREWO_6$ (RE = La, Pr, Gd, and Dy).

spectra [21,22]. Samples of Aurivillius family of layered perovskites of various chemical compositions, $BiREWO_6$ (RE = Y, Nd,and Gd), crystallize in a monoclinic lattice with $A12/m1$ space group [16]. A total number of vibrational modes at the center of the Brillouin zone of this space group were divided into the irreducible representations as

$$\Gamma = 24A_g + 18A_u + 18B_g + 24B_u$$

Out of these, A_g and B_g irreducible representations correspond to Raman active modes, whereas A_u and B_u are infrared active. The FT-IR spectra of all the compounds were recorded in the range of 4000–400 cm^{-1} (Fig. S5). These spectra were comparable with the FT-IR spectra of $BiREWO_6$ (RE = Nd, Gd, and Y) [16]. The FT-IR spectral profiles of $BiREWO_6$ (RE = La, Pr, Gd, and Dy) are similar to each other. The absorption band around 3500 cm^{-1} for $BiPrWO_6$ is may be due to surface O–H groups. The small shift in the position of FT-IR bands for $BiREWO_6$ (as shown in Fig. S5) may be correlated to the ionic radius of RE^{3+}. As the ionic radius of RE^{3+} is small, the Bi/RE atoms are more tightly bound to oxygen atoms and results in a decrease in the Bi/RE–O bond length. A decrease in the bond length leads to a higher force constant and hence higher vibrational frequency. All the FT-IR band positions for these samples are given in Table S3.

The optical characteristics of the samples are comprehended from diffuse reflectance spectra recorded in the range of 200–900 nm. Fig. 4 shows the absorption spectra of $BiREWO_6$. All the samples had strong absorption bands in the 380–400 nm region. The less intense bands observed in the visible region for $BiPrWO_6$ and $BiDyWO_6$ are attributed to f–f electronic transitions of the Pr^{3+} and Dy^{3+} ions. The absorption values at the edge of $BiLaWO_6$, $BiPrWO_6$, $BiGdWO_6$, and $BiDyWO_6$ were found to be 556, 510, 503, and 525 nm, respectively. In general, the band gap energy (E_g) of the semiconductor material is related to its band edge position. The relative shift in the absorption edge of the semiconductor depends strongly on the difference between the ionic radius of the dopant and the host cations as well as on the chemical nature of the dopants. The corresponding band gap energy for these samples was obtained from the plot of $(Kh\nu)^{1/2}$ versus $h\nu$, where K is reflectance transformed according to the Kubelka–Munk plot [$K = (1-R)^2/2R$, R is the reflectance (%)] and $h\nu$ is the photon energy. Extrapolation of the linear portion of the plot to $(Kh\nu)^{1/2} = 0$ (i.e., onto the x-axis) gives an estimation of band gap energy (Fig. S6) [23]. The deduced band gap energy values of $BiLaWO_6$, $BiPrWO_6$, $BiGdWO_6$, and $BiDyWO_6$ were 2.23, 2.43, 2.46, and 2.36 eV, respectively.

The compositions investigated in this study are expected to exhibit visible light photocatalytic activity due to their narrow band gap. To explore the visible light catalytic activity of $BiREWO_6$ (RE = La, Pr, Gd, and Dy), methylene blue (MB) was taken as the model pollutant. MB is widely used in textile industry as a dyeing agent. It is toxic, so the effluent water has to be treated before it is discharged into natural water streams. The visible light photodegradation behavior of MB in the presence of all the samples was investigated. Before the visible light irradiation, all the samples were kept in the dark chamber for 1 h to attain adsorption–desorption equilibrium between the solid catalyst and MB aqueous solution. The degradation of all samples was monitored by measuring the optical density (at 664 nm) and the UV–vis spectra at different time intervals of visible irradiation. The absorption spectrum of MB was characterized by a medium band at ~300 nm and a strong band at ~675 nm with a shoulder at ~600 nm. The band at 300 nm arises due to the aromatic ring while the overlapping bands are assigned to conjugated π-system [24]. It was observed from the UV–vis absorption spectrum of MB that the degradation of MB increased with increase in the irradiation time and all the materials in the present investigation have exhibited photoactivity against MB degradation under visible light irradiation (representative UV–vis absorption spectrum of MB in the presence of $BiGdWO_6$ is given in Fig. S7). The temporal change in the concentration of MB measured by following the variations in maximal absorption in the UV–vis spectra is shown in Fig. 5. For the 180 min of visible light irradiation, the degraded amounts of MB were found, respectively, to be 78%, 74%, 92%, and 70% in the presence of $BiLaWO_6$,

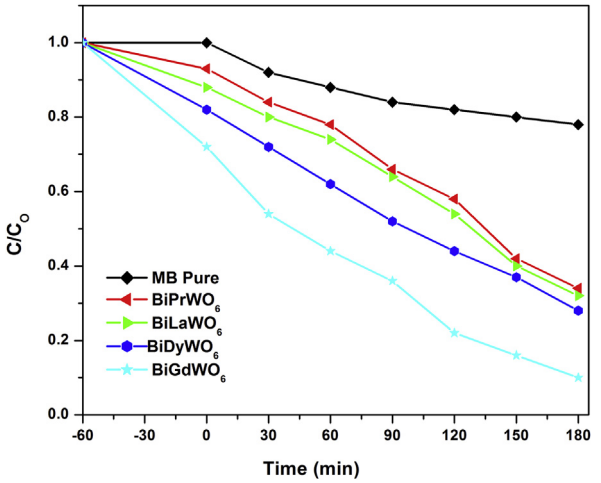

Fig. 5. Temporal changes in the MB concentration in the absence and presence of BiREWO$_6$ (RE = La, Pr, Gd, and Dy) under the visible light irradiation.

$BiPrWO_6$, $BiGdWO_6$, and $BiDyWO_6$. It is also observed that 22% of MB was almost degraded without catalyst after 180 min. This is due to the self-photolysis of MB.

It is well established that the band gap energy of the material, holes formation, and photogenerated electron–hole pair recombination rate during the photocatalytic reaction play a significant role in the dye degradation process [25]. The photogenerated electron–hole pairs produce hydroxyl and superoxide radicals, respectively, on reacting with catalyst surface adsorbed H_2O and O_2. These radicals successively degrade the dye molecules into harmless inorganic molecules such as CO_2 and H_2O. The typical degradation pathway of the MB dye in the presence of catalysts is given below

$$BiREWO_6 + h\nu \rightarrow e^-_{cb} + h^+_{vb}$$
$$H_2O + h^+_{vb} \rightarrow {}^{\cdot}OH + H^+$$
$$O_2 + e^-_{cb} \rightarrow O_2{}^{\cdot -}$$
$$O_2{}^{\cdot -} + H^+ \rightarrow HO_2{}^{\cdot}$$
$$2HO_2{}^{\cdot} \rightarrow H_2O_2 + O_2$$
$$H_2O_2 \rightarrow 2OH^{\cdot}$$
$${}^{\cdot}OH, O_2{}^{\cdot -}, h^+_{vb} + MB \rightarrow Byproducts$$

In the present work, the formation of holes, hydroxyl radicals, and superoxide radicals during MB degradation has been experimentally verified using radical quenchers.

As conferred above, the photocatalytic degradation of organic pollutes predominantly depend on the production of reactive species including hydroxyl radicals, very powerful chemical oxidants, which can destroy a wide range of resilient organic pollutants [26–30]. The generation of ·OH radicals is mainly due to the oxidation of surface water by the holes, which are escaped in the rapid carrier recombination process. Hence, a greater rate of formation of ·OH radicals corresponds to higher separation efficiency of electron–hole pairs, which lead to a higher photocatalytic activity. The production of ·OH in the presence of all the oxides during the irradiation is further demonstrated by a fluorescence technique using TA as a probe. The generated ·OH species during the photoreaction react with TA to give TAOH, which has a characteristic fluorescence signal at 426 nm. Higher emission intensity at 426 nm over catalyst signals higher concentration of ·OH (or formation of TAOH). The fluorescence intensity at 426 nm of a TA solution in the presence of all the catalysts is found to increase with the increase in visible light irradiation time. However, the fluorescence intensity is higher in the presence of $BiGdWO_6$ as compared to $BiLaWO_6$, $BiPrWO_6$, and $BiDyWO_6$ (Fig. 6). The very low emission intensity of $BiPrWO_6$ and $BiDyWO_6$ can be attributed to higher electron–hole pair recombination during the photoreaction. It was further evidenced by recording their photoluminescence (PL) spectra, which have been widely used to investigate the efficiency of charge carrier migration, trapping, and transfer to understand the fate of electron–hole pairs in semiconductors [26]. It is also expected that the rare earth ion–containing materials exhibit photoemission and absorption properties because of electric and magnetic optical transitions within their 4f states. The higher PL intensity of $BiPrWO_6$ and $BiDyWO_6$ indicates a higher recombination rate, which implies the lower rate of formation of ·OH radicals and hence lower photodegradation rate (Fig. 6). The PL for $BiGdWO_6$ and $BiLaWO_6$ was not observed and hence not shown in Fig. S8. The higher photodegradation of MB in the presence of $BiGdWO_6$ as compared to the rest of the materials can be endorsed to its high ·OH radical generation.

To investigate the participation of holes (h^+), hydroxyl (·OH) radicals, and super oxide ($O_2{}^{\cdot -}$) radicals in the photocatalytic degradation of MB in the presence of $BiGdWO_6$, competitive reactions using radical quenchers were carried out. Ammonium oxalate, isopropyl alcohol (*i*-PrOH), and benzoquinone were used to quench the holes (h^+), hydroxyl ·OH radicals, and superoxide ($O_2{}^{\cdot -}$) radicals, respectively. The photodegradation of MB was carried out by adding individually 2 mM of ammonium oxalate, 2 mM of *i*-PrOH, and 2 mM of benzoquinone to the $BiGdWO_6$ catalyst under identical conditions. As shown in Fig. S9, the

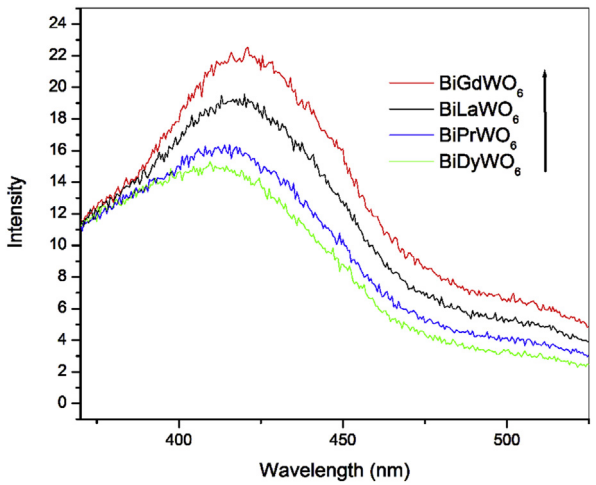

Fig. 6. PL spectra of TA in the presence of BiREWO$_6$ (RE = La, Pr, Gd, and Dy) at 180 min of visible light irradiation.

MB degradation is reduced noticeably by the addition of quenchers. On the basis of these results, it was understood that holes (h^+), hydroxyl $^{\cdot}OH$ radicals, and super oxide ($O_2^{\cdot -}$) radicals participated significantly in the photocatalytic degradation of MB.

4. Conclusions

$BiREWO_6$ (RE = La, Pr, Gd, and Dy) were prepared by the sol–gel method. All the samples were crystallized in a monoclinic lattice with space group $A12/m1$. The Raman spectral profiles of $BiREWO_6$ (RE = La, Pr, Gd, and Dy) are similar to each other, except changes in intensity, line width, and positions of the bands. The deduced band gap energy values of $BiLaWO_6$, $BiPrWO_6$, $BiGdWO_6$, and $BiDyWO_6$ were 2.23, 2.43, 2.46, and 2.36 eV, respectively. The degraded amounts of MB were found to be, respectively, 78%, 74%, and 70%, and 92% over $BiLaWO_6$, $BiPrWO_6$, $BiGdWO_6$, and $BiDyWO_6$ for 180 min of visible light irradiation. The production of $^{\cdot}OH$ in the presence of catalysts during the irradiation was confirmed by fluorescence technique using TA as the probe. The higher photodegradation of MB in the presence of $BiGdWO_6$ as compared to the rest of the materials can be endorsed to its high $^{\cdot}OH$ radical generation. On the basis of the competitive photocatalytic reactions using scavengers, it was understood that holes (h^+), hydroxyl ($^{\cdot}OH$) radicals, and super oxide ($O_2^{\cdot -}$) radicals play a pivotal role in the photocatalytic degradation of MB.

Acknowledgments

The authors would like to acknowledge CSIR, New Delhi, under the CSIR-scheme (No. 01(2857)/16/EMR-II) and the UGC, New Delhi, under UPE-FAR (14-5/2012 (NS/PE)) Programme for their financial support. M.V. thanks, UGC, New Delhi for the award of BSR fellowship.

Appendix A. Supplementary data

Supplementary data related to this article can be found at https://doi.org/10.1016/j.crci.2018.01.011.

References

[1] H. He, S.P. Berglund, A.J.E. Rettie, W.D. Chemelewski, P. Xiao, Y. Zhang, C. Buddie Mullins, J. Mater. Chem. 2 (2014) 9371–9379.
[2] B.J. Trześniewski, W.A. Smith, J. Mater. Chem. 4 (2016) 2919–2926.
[3] Z. Liu, F. Chen, Y. Gao, Y. Liu, P. Fang, S. Wang, J. Mater. Chem. 1 (2013) 7027–7030.
[4] P. Dong, Y. Wang, H. Li, H. Li, X. Ma, L. Han, J. Mater. Chem. 1 (2013) 4651–4656.
[5] H. Hongyan, J. Zhengbo, Y. Hongchao, L. Gongxuan, Y. Jinhua, B. Yingpu, J. Mater. Chem. 1 (2013) 2387–2390.
[6] X. Hui, L. Huaming, L. Xu, W. Chundu, S. Guang, Song Yuanguo Xu, J. Chu, Ind. Eng. Chem. Res. 48 (2009) 10771–10778.
[7] H. Li, S. Yin, Y. Wang, T. Sekino, S.W. Lee, T. Sato, J. Mater. Chem. 1 (2013) 1123–1126.
[8] S. Pasternak, Y. Paz, J. Photochem. Photobiol., A 318 (2016) 14–24.
[9] R. Shi, G. Huang, J. Lin, Y. Zhu, J. Phys. Chem., C 113 (2009) 19633–19638.
[10] H. Liu, J. Yuan, W. Shang guan, Y.S. Teraoka, J. Phys. Chem. C 112 (2008) 8521–8523.
[11] H. Fu, C. Pan, W. Yao, Y. Zhu, J. Phys. Chem. B 109 (2005) 22432–22439.
[12] H. Fu, W. Yao, L. Zhang, Y. Zhu, Appl. Catal., B 66 (2006) 100–110.
[13] S. Murugesan, M.N. Huda, Y. Yan, M.M. Al-Jassim, B.V.R. Subramanian, J. Phys. Chem. C 114 (2010) 10598–10605.
[14] S. Gupta, L. De Leon, V. R. Subramanian, Phys. Chem. Chem. Phys. 16 (2014) 12719–12727.
[15] N. Santha, P. Koshy, M.T. Sebastian, J. Mater. Sci.: Mater. Electron. 13 (2002) 229–232.
[16] P.S. Berdonosov, D.O. Charkin, K.S. Knight, K.E. Johnston, R.J. Goff, V.A. Dolgikh, P. Lightfoot, J. Solid State Chem. 179 (2006) 3437–3444.
[17] R.D. Shannon, C.T. Prewitt, Acta Crystallogr. B 25 (1969) 925–946.
[18] A. Watanabe, Z. Inoue, T. Ohsaka, Mater. Res. Bull. 15 (1980) 397–404.
[19] A. Watanabe, Mater. Res. Bull. 15 (1980) 1473–1477.
[20] A. Watanabe, Y. Sekikawa, F. Izumi, J. Solid State Chem. 41 (1982) 138–142.
[21] H. AitAhsaine, A. Taoufyq, L. Patout, M. Ezahri, A. Benlhachemi, B. Bakiz, S. Villain, F. Guinneton, J.R. Gavarri, J. Solid State Chem. 218 (2014) 124–130.
[22] M. Maczka, J. Hanuza, W. Paraguassu, A.G. Souza, P.T.C. Freire, J.M. Filho, Appl. Phys. Lett. 92 (2008) 112911–112913.
[23] G. Ravi, P. Suresh, V. Naveen Kumar, J.R. Reddy, A. Hari Padmasri, M. Vithal, Int. J. Hydrogen Energy 39 (2014) 15352–15361.
[24] G. Ravi, P. Suresh, J.R. Reddy, V.N. Kumar, B. Vijaya Kumar, M. Vithal, Int. J. Green Nanotechnol. 4 (2012) 360–367.
[25] A. Hegazy, E. Prouzet, C. R. Chimie 16 (2013) 651–659.
[26] K. Yamada, H. Nakamura, S. Matsushima, H. Yamane, T. Haishi, K. Ohira, K. Kumada, C. R. Chimie 9 (2006) 788–793.
[27] R. Murugan, L. Kashinath, R. Subash, P. Sakthivel, K. Byrappa, S. Rajendran, G. Ravi, Mater. Res. Bull. 97 (2018) 319–325.
[28] R.S. Ganesh, E. Durgadevi, M. Navaneethan, S.K. Sharma, H.S. Binitha, S. Ponnusamy, C. Muthamizhchelvan, Y. Hayakawa, Chem. Phys. Lett. 684 (2017) 126–134.
[29] M. Dhanasekar, S. Ratha, C.S. Rout, S.V. Bhat, J. Environ. Chem. Eng. 5 (2017) 2997–3004.
[30] C.H. Sudhakar Reddy, K. Sreenu, J.R. Reddy, A. Hari Padmasri, G. Ravi, M. Vithal, J. Chem. Sci. 128 (2016) 663–670.